Research Article Vol. 15, No. 12 / 1 Dec 2025 / Optical Materials Express 3289
Optical Materials EXPRESS

# Quantitative analysis of chalcogenide glass aging in flexible photonic devices

YINGCHUN WU,[1,2,3] YILIN SHI,[2,3] KAI XU,[4] ZEQUN CHEN,[2,3] MAOLIANG WEI,[4] KANGJIAN BAO,[2,3] YE LUO,[2,3] RENJIE TANG,[2,3] HAOMIN WANG,[2,3] BOSHU SUN,[2,3] CHUNLEI SUN,[2,3] WEI ZHANG,[5] HONGTAO LIN,[4] AND LAN LI[2,3,6,*]

[1]*Zhejiang University, Hangzhou 310058, China*
[2]*Zhejiang Key Laboratory of 3D Micro/Nano Fabrication and Characterization, Department of Electronic and Information Engineering, School of Engineering, Westlake University, Hangzhou 310030, China*
[3]*Institute of Advanced Technology, Westlake Institute for Advanced Study, Hangzhou 310024, China*
[4]*MOE Frontier Science Center for Brain Science & Brain-Machine Integration, Key Laboratory of Micro-Nano Electronics and Smart System of Zhejiang Province, College of Information Science and Electronic Engineering, Zhejiang University, Hangzhou, Zhejiang 310027, China*
[5]*Zhejiang Key Laboratory of Advanced Optical Functional Materials and Devices, Faculty of Electrical Engineering and Computer Science, Ningbo University, Ningbo 315211, China*
[6]*Westlake Institute for Optoelectronics, Fuyang, Hangzhou 311400, China*
[*]*lilan@westlake.edu.cn*

**Abstract:** Chalcogenide glass (ChG) shows significant promise for applications in flexible integrated photonics due to its excellent optical properties and monolithic integration capability. However, the long-term stability of chalcogenide materials remains a critical challenge, limiting the broader deployment of device applications. To date, there has been limited research focused on flexible photonic devices fabricated from Ge-Sb-Se-based ChGs, particularly regarding their aging behavior and mechanical robustness under operational conditions. To address this, we employed the resonant refractometry method to investigate the aging process of Ge-Sb-Se ChG in flexible integrated photonic devices. Our experimental results reveal that thermal annealing plays a significant role in accelerating the aging behavior of ChG devices. Devices that underwent thermal annealing demonstrated enhanced stability, suggesting that thermal annealing serves as an effective approach to accelerate the aging process in optical performance. Additionally, we showed that the flexible devices retained their excellent mechanical stability even after undergoing thermal annealing. The findings of this study offer insights into strategies for improving the long-term stability of Ge-Sb-Se-based photonic devices.



## 1. Introduction

Flexible integrated photonic devices hold significant promise for optical sensing applications due to their unique advantages. For example, flexible photonics extends the mechanical adaptability of optical systems [1], enabling conformal integration on non-planar and dynamic surfaces [2,3]. Compared to flexible electronics, photonic systems offer higher bandwidth [4] and reduced crosstalk [5], while their high multiplexing capacity [6,7] allows for compact, space-efficient designs [8]. In contrast to optical fibers, flexible photonic devices provide greater geometric versatility [9,10] and stronger optical confinement [11], facilitating enhanced light–matter interactions within compact space. Advances in monolithic integration [9,12,13] have further enabled the scalable fabrication of flexible photonic circuits. Among candidate materials, chalcogenide glasses (ChGs) exhibit exceptional optical properties, including broad infrared transparency [14,15], nonlinear properties [16,17], and fabrication compatibility with CMOS back-end-of-line processes [18,19], making them well suited for applications in photonic integrated

#580588 https://doi.org/10.1364/OME.580588
Journal © 2025 Received 1 Oct 2025; revised 16 Nov 2025; accepted 18 Nov 2025; published 1 Dec 2025

Optical Materials EXPRESS

circuits (PICs) [20,21] for applications in mid-infrared sensing [22,23], optical interconnects [24] and nonlinear optics [25,26]. In particular, germanium (Ge)-antimony (Sb)-selenium (Se)-based ChGs are widely used for fabricating flexible integrated photonic devices due to their high refractive index (2.60-2.80) [27] and low propagation loss (0.8 dB $cm^{-1}$) [28]. Moreover, these materials can be deposited at room temperatures [1,29,30], enabling monolithic integration on flexible substrates.

Glass materials, including ChGs, exhibit intrinsic aging at room temperature [31–34], which can compromise the long-term reliability of sensing applications. Understanding their aging behavior is therefore crucial to ensure stable and reliable performance of ChG-based photonic devices. The fundamental origins of aging [31] are complex and not yet fully understood. For example, hydrolysis reactions between sulfur-containing groups and water have been identified as the primary driver of compositional changes in ChGs [32], while defect migration further accelerates structural instability [35]. Additionally, surface oxidation caused by oxygen diffusion has been shown to reduce infrared transmittance, thereby limiting device performance [36]. Despite the progress made in understanding these processes, existing research primarily focuses on the aging of bulk materials [27,33] and thin films [36]. However, the aging of functional ChG photonic devices in a practical sensing application remains uncertain. Previous studies have shown the effect of temperature on the refractive index and extinction coefficient over a wide spectral range for selected bulk ChGs [27]. Although Hu et al. investigated the aging of Ge–Sb–S ChG microring resonator devices in 2019 [37] and showed that thermal annealing stabilizes optical performance more effectively than photo-saturation, the results were analyzed based on a rigid substrate, leaving the behavior in flexible devices unexplored.

In our study, we selected Ge–Sb–Se ChG for our flexible integrated photonic devices due to its higher refractive index [38] and broader infrared transparency window [39,40] compared to Ge–Sb–S ChGs. We investigated the performance evolution of Ge-Sb-Se ChGs photonic devices under operational aging, particularly regarding the influence of thermal annealing on flexible photonic systems. The aging process was monitored by tracking the resonant wavelength shifts in the side-coupled one-dimensional photonic crystal microcavities. Since the resonant wavelength shift can be used to extrapolate the refractive index change of the ChG [37]. Under well-controlled environmental conditions, the study focused on the effect of annealing treatment on the accelerated aging process. The optical properties and mechanical robustness of the annealed devices were further assessed before and after transfer to a flexible substrate. The results demonstrated that the annealed devices retain mechanical integrity and exhibited minimal degradation in optical performance after transfer and bending. This technique enables the assessment of aging under conditions representative of actual integrated photonic device operation, ensuring direct relevance to real-world flexible sensing applications. The findings offer practical guidance for improving the long-term stability of photonic devices based on Ge-Sb-Se ChG materials, thereby facilitating the development of more reliable and robust flexible integrated photonic sensors.

## 2. Material, structure and design, fabrication and testing

### 2.1. Material

Integrated photonic circuits based on ChGs are commonly used in a diverse range of sensing applications [41–45]. In this study, $Ge_{28}Sb_{12}Se_{60}$ (GSSe) was chosen as the material of choice for designing and fabricating photonic crystal devices [46–48]. The refractive index of thermally evaporated GSSe film is approximately 2.68 at 1550 nm, as shown in Fig. 1.

### 2.2. Structure and design

The proposed photonic device is based on a side-coupled one-dimensional (1D) photonic crystal microcavity, also known as a Bragg grating-based Fabry–Pérot (F–P) cavity. This structure

Optical Materials EXPRESS

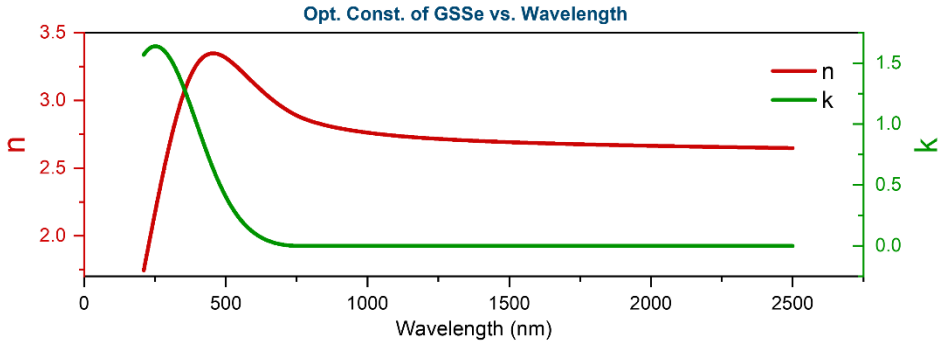


**Fig. 1.** Measurement of the refractive index and extinction coefficient of the GSSe film by thermal evaporation deposition process.

consists of two distributed Bragg gratings, tapered transition regions, and a central single-mode waveguide, as schematically illustrated in Fig. 2(a). The side-coupled configuration enables integration with a curved waveguide, allowing for compact and scalable cascading of multiple microcavity units. To ensure single-mode operation, numerical simulations were performed to determine the optimal waveguide dimensions. For a core thickness of 300 nm, modal analysis confirmed that a waveguide width of 700 nm supports only the fundamental transverse electric (TE) mode, as shown in Fig. 2(b). Furthermore, simulation results confirm that the cavity supports a single resonant mode (Fig. 2(c)) across a wide wavelength range of 200 nm, from 1400 nm to 1600 nm. By adjusting the Bragg grating period, the resonant wavelength can be precisely tuned within a spectral window of 1400-1600 nm (Fig. S1). This leads to a significantly extended free spectral range (FSR), which is essential for enabling multi-point sensing in a wavelength division multiplexing (WDM) configuration. The design not only enhances the sensing capability but also improves the system's integration potential [8].

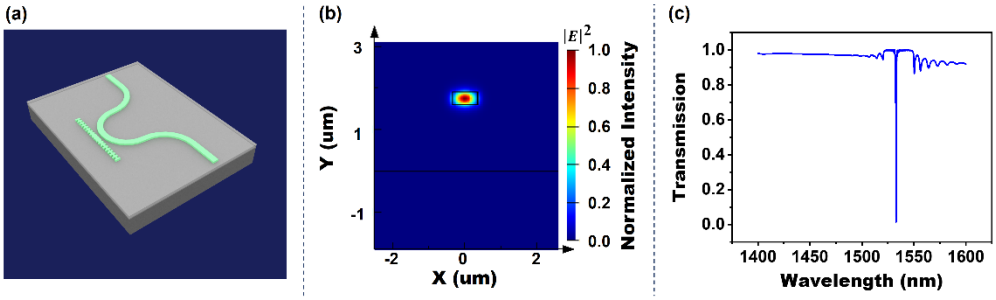


**Fig. 2.** (a) 3D perspective drawing of the schematic design of a 1D photonic crystal microcavity. (b) TE mode profiles for a 700 nm-width waveguide, GSSe as core material, and SU-8 as cladding. (c) Calculated transmission of the designed microcavity in the wavelength range of 1400-1620 nm.

### 2.3. *Fabrication and testing*

Figure 3 presents a schematic illustration of the fabrication process for the GSSe devices used in aging measurements. As an amorphous material, GSSe can be directly deposited via low-temperature thermal evaporation (below 350 °C [49]). A 300 nm-thick GSSe film was deposited onto a lower cladding layer of SU-8 (2 μm). The base pressure was evacuated down to $5 \times 10^{-4}$ Pa when deposition. A side-coupled 1D photonic crystal microcavity was then fabricated

Optical Materials EXPRESS

on the ChG film using electron-beam lithography and plasma etching, ensuring a clean and contamination-free surface for high-quality device performance. SU-8 photosensitive resin is used as both the top and bottom cladding materials. The cladding layers are fabricated through standard photolithography and thermal curing processes, forming a symmetrical waveguide structure that effectively isolates the device from environmental humidity.

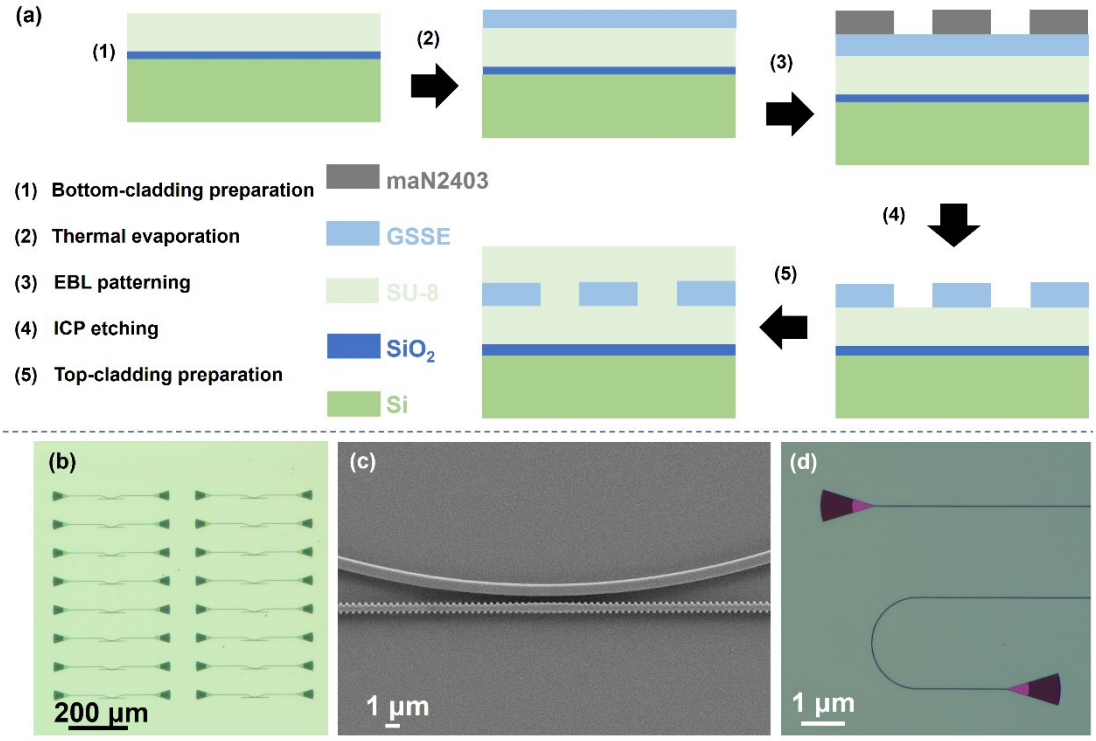


**Fig. 3.** (a) Fabrication process of the GSSe side-coupled 1D photonic crystal microcavity. (b) Optical microscope image of the devices. (c) SEM of the side-coupled 1D photonic crystal microcavity. (d) Optical microscope image of the grating coupler.

The effect of thermal annealing on the aging behavior of GSSe ChG was investigated by monitoring two groups of devices: a blank control group (Devices 1–8) and a thermally treated group (Devices A–H). The control group received no additional treatment, while the treated group was annealed at 250 °C [50] for 2 hours in a nitrogen-protected oven. Subtle resonance peak shifts are monitored to accurately track the structural changes associated with the aging process of the GSSe film, enabling high-resolution aging analysis under controlled conditions. During the measurement process, all devices were placed in a light-shielded environment to eliminate any influence of ambient illumination (considering the photosensitivity [16]). The aging behavior was observed over two distinct time intervals: a short-term period (0–7 hours) and an extended duration (0–168 hours).

All aging measurements were performed in a controlled environment maintained at room temperature (22.0 ± 0.5 °C), minimizing external thermal variations. Consequently, the influence of ambient temperature fluctuation on the observed aging-induced wavelength shifts was negligible, enabling a more accurate evaluation of the intrinsic aging behavior of GSSe ChGs.

Optical Materials EXPRESS

## 3. Results and discussion

### 3.1. Aging evaluation

The unannealed control devices were first studied to understand intrinsic aging before assessing how thermal annealing affects aging behavior and optical stability. In this experiment, no annealing treatment was applied, and resonance peak monitoring of the microcavities was initiated immediately after fabrication. The results are shown in Fig. 4(a), which displays the aging behavior of Devices 1–8 over a 7-hour observation period (measured hourly). A distinct red shift in the resonance wavelength was observed (Supplement 1, Fig. S2), indicating an increase in the effective index of the device resonator due to the aging of ChG glass over time. All devices exhibited a consistent resonance wavelength shift of 671 ± 16 pm within a 7-hour observation aging period. The aging rates varied slightly among devices, indicating some degree of device-dependent instability. Since no significant reduction in the resonant shift rate was observed, Devices 1–4 were monitored at additional 0-48, 48-104, and 104-168-hour intervals to evaluate aging progression over an extended duration. After 168 hours of observation, these devices exhibited red shifts in resonance wavelength with a mean value of 1312 ± 126 pm. The observed red shift in the resonance wavelength is consistent with structural relaxation in chalcogenide glasses. This behavior is discussed in detail in the Supplement 1 (Fig. S3). The results show that the rate of resonance peak shift gradually decreases with increasing aging time, indicating a deceleration of the aging process over time, as illustrated in Fig. 4(b). Notably, by 104 hours, the shift rate had dropped to less than 20% of the initial rate, suggesting that the material undergoes a progressive stabilization phase during prolonged aging. The resonant wavelength shift reported here is directly proportional to the refractive index change of the GSSe film. Future work will involve detailed optical simulations to extract the exact confinement factor, enabling the presentation of data in refractive index change units for broader applicability.

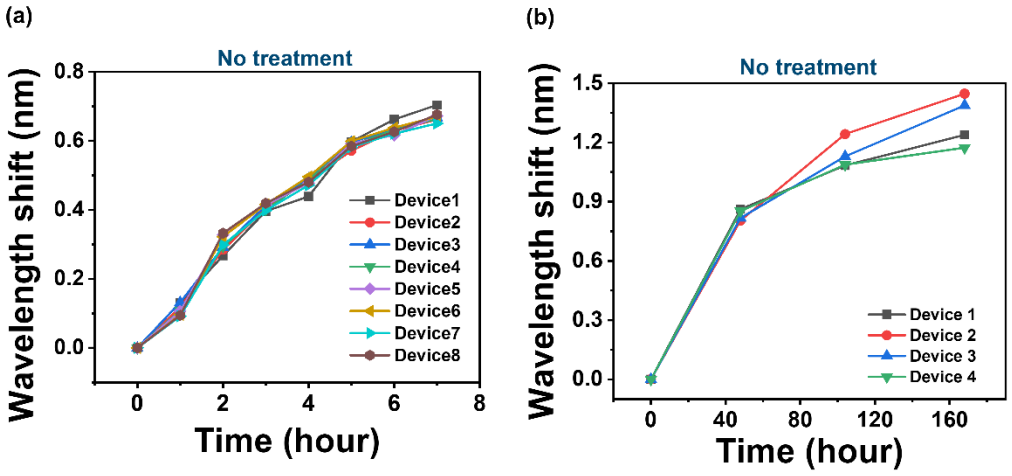


**Fig. 4.** Temporal aging-induced resonance wavelength shifts in untreated flexible ChG resonators. (a) Short-term evolution observed within the first 7 hours post-fabrication, highlighting the initial rapid shift phase. (b) Long-term evolution over 168 hours, illustrating the progression towards relative stability.

A comparative study was conducted to assess the effect of thermal annealing on the aging behavior of ChG devices. A second set of eight devices (Devices A–H) was annealed at 250 °C for 2 hours in a nitrogen-protected environment. The resonance peak shifts of the annealed devices were subsequently monitored over both short-term (0–7 hours) and long-term (up to 168

Optical Materials EXPRESS

hours) periods. The results are presented in Fig. 5(a) and (b), respectively. Quantitative analysis revealed that, after 7 hours of aging, the annealed devices exhibited a red shift in resonance wavelength, ranging from 254 pm (minimum) to 421 pm (maximum), with a mean shift of 341 ± 61 pm—approximately 50% of the average shift observed in the non-annealed control group. Extending the observation period to 168 hours revealed that Devices A–D exhibited a mean resonance peak shift of 729 ± 25 pm, approximately half of that measured in the untreated samples. These consistent reductions in resonance peak shifts across both time scales clearly demonstrate that thermal annealing significantly accelerates the aging process, driving the devices toward a more stable optical state at an earlier stage. The substantially smaller shifts observed in both short-term and long-term measurements, compared to those of the non-annealed devices, suggest that thermal treatment promotes a faster stabilization of the material's optical properties.

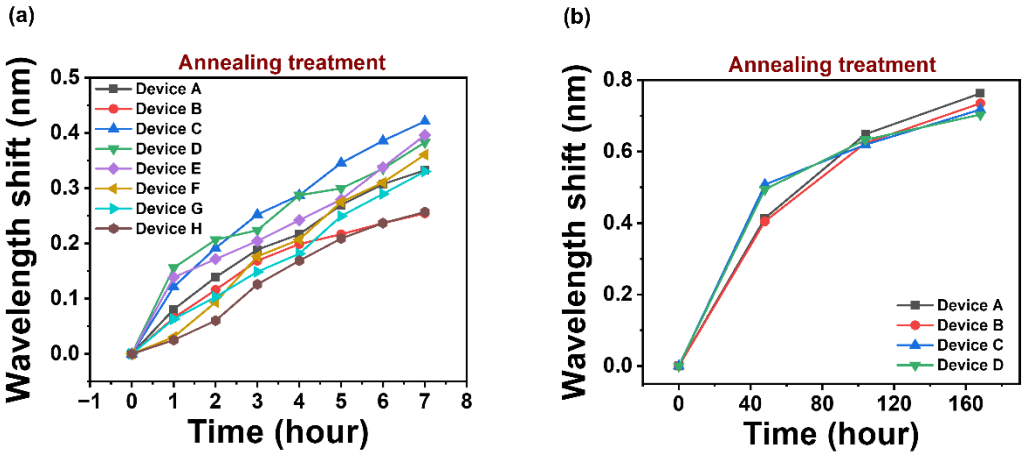


**Fig. 5.** Temporal aging-induced resonance wavelength shifts in thermally treated (250 °C, 2 hours) flexible ChG resonators. (a) Short-term evolution observed within the first 7 hours post-fabrication, highlighting the initial rapid shift phase. (b) Long-term evolution over 168 hours, illustrating the progression towards relative stability.

Based on the comparison results of the untreated (devices 1-4) and annealed (devices A-D, 250 °C, 2 hours) device groups, the evolution of aging rates in the three characteristic time intervals of 0-48 hours, 48-104 hours, and 104-168 hours was statistically analyzed. Figure 6 presents the time evolution during aging of four representative devices in each treatment group, and quantitatively compares the statistical aging rates between the two groups. The results of the statistical analysis indicate that, after annealing treatment, the effect of accelerated aging is not evident in the early stage (0-48 hours), but becomes apparent in the middle stage (48-104 hours). The shift rate of the resonant peak significantly slowed down, approximately 1/5 of that of the untreated device. In the later stage (104-168 hours), it gradually stabilized, and the shift rate of the resonant peak began to approach zero. Presenting this comparative analysis provides quantitative insights into how annealing affects aging kinetics across different stages of the stabilization process.

### 3.2. *Performance of the flexible device*

The optical performance under mechanical deformation was monitored through controlled experiments. First, annealed devices were carefully delaminated from their rigid silicon substrates and transferred to flexible polyimide (PI) substrates using an optimized transfer process (Fig. 7(a)). The detailed transfer process information is demonstrated in Supplement 1 and Fig.

Optical Materials EXPRESS

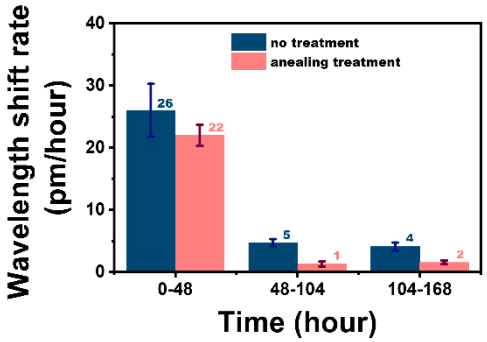


**Fig. 6.** Resonance wavelength shift rate comparison between annealed and unannealed devices during aging

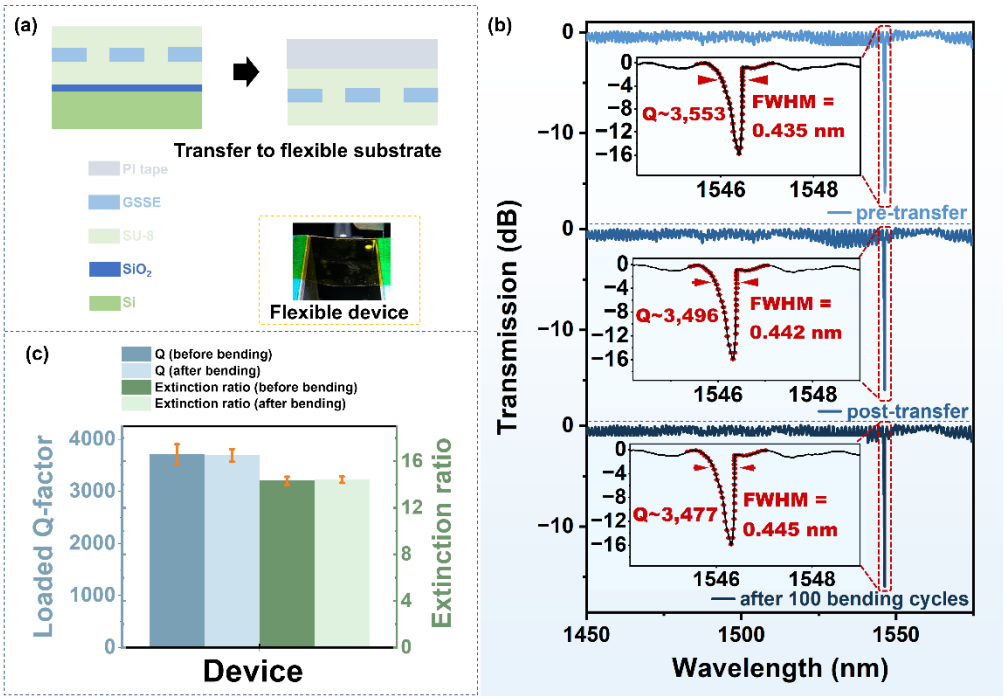


**Fig. 7.** (a) Schematic drawing of the flexible transferring process and physical picture of flexible device. (b) Optical performance of Device A on a rigid substrate, after transferring to a flexible substrate, and after 100 bending cycles. (c) Loaded Q-factors and extinction ratios of devices with annealing treatment before and after 100 bending cycles (statistical results of device A~D).

S4. Comprehensive optical characterization was then performed on four representative devices at three key stages: (1) pre-transfer, (2) post-transfer, and (3) after repeated bending cycles (Fig. 7(b)). During the bending tests, the devices were subjected to 100 cycles of mechanical deformation under a bending radius of 1 mm, simulating demanding operational conditions. Our comparative spectral analysis revealed excellent mechanical stability of the device. The extinction ratio varied by less than 1 dB, and the quality factor (Q-factor) decreased by less than 3% after 100 bending cycles (Fig. 7(c)). These results provide strong evidence that the thermal

Optical Materials EXPRESS

annealing process not only improves aging stability, as previously demonstrated, but also enables the realization of flexible photonic devices that maintain outstanding optical performance under significant mechanical stress. The minimal degradation observed in both extinction ratio and Q-factor conclusively demonstrates that the annealed ChG devices retain exceptional structural integrity and optical functionality under substantial mechanical deformation.

## 4. Conclusion

In conclusion, we have quantitatively evaluated the aging behavior of ChGs in flexible photonic devices through the resonant cavity refractometry technique. The devices, based on a side-coupled 1D photonic crystal microcavity fabricated using GSSe glass as the core material, enable high-resolution analysis of refractive index for device aging study. Our results demonstrate that thermally annealed devices show a significantly slower resonance peak shift rate compared to untreated counterparts, indicating that controlled thermal treatment effectively enhances the long-term stability of flexible integrated photonic devices based on ChG. Furthermore, we proved that the annealing process does not compromise the mechanical robustness of the flexible device. The minimal degradation in extinction ratio (<1 dB) and quality factor (<3%) after 100 bending cycles under a 1 mm curvature radius conclusively confirms that annealed ChG devices maintain exceptional structural integrity and optical performance under mechanical deformation. These findings validate their suitability for mechanically demanding flexible photonic applications. This study further supports the effectiveness of resonance peak shift monitoring as a reliable and sensitive method for assessing the aging performance of ChG-based photonic devices. While the current work focuses on GSSe-based microcavities, the methodology can be extended to other glass compositions and device architectures to explore the generality of the observed aging behavior and thermal stabilization effects.

**Funding.** National Natural Science Foundation of China (62175202); "Pioneer" and "Leading Goose" Research and Development Program of Zhejiang Province (2024SDXHDX0005); Key Research and Development Program of Zhejiang Province (2024C03150); Key Project of Westlake Institute for Optoelectronics (2023GD003/110500Y0022303).

**Acknowledgments.** The authors would like to acknowledge the Westlake Center for Micro/Nano Fabrication and ZJU Micro-Nano Fabrication Center at Zhejiang University for the facility support. Furthermore, the authors thank Mr. Xi Mu for his assistance with E-beam evaporation deposition. They also express appreciation to Xinyu Qiao for his help with GSSe film preparation and to Yuxiang Zeng for her assistance with transmission spectrum characterization.

**Disclosures.** The authors declare no conflicts of interest.

**Data availability.** Data underlying the results presented in this paper are not publicly available at this time but may be obtained from the authors upon reasonable request.

**Supplemental document.** See Supplement 1 for supporting content.

## References

1. Y. Wu, K. Bao, J. Liang, *et al.*, "Photonic Interfaces: an Innovative Wearable Sensing Solution for Continuous Monitoring of Human Motion and Physiological Signals," Small Methods **27**, 2500727 (2025).
2. Y. Zhang, J. Reddy, M. Chamanzar, *et al.*, "A Novel Parylene C Waveguide-Based High-Resolution Photonic Tactile Array Sensor," Adv. Mater. Technol. **10**(5), 2400752 (2025).
3. Y. Luo, C. Sun, M. Wei, *et al.*, "Integrated Flexible Microscale Mechanical Sensors Based on Cascaded Free Spectral Range-Free Cavities," Nano Lett. **23**(19), 8898–8906 (2023).
4. G. Terrasanta, M. W. Ziarko, N. Bergamasco, *et al.*, "Photonic Integrated Circuits for Optical Satellite Links: A Review of the Technology Status and Space Effects," Satell. Commun. Network **43**(3), 210–228 (2025).
5. F. Ceccarelli, S. Atzeni, C. Pentangelo, *et al.*, "Low Power Reconfigurability and Reduced Crosstalk in Integrated Photonic Circuits Fabricated by Femtosecond Laser Micromachining," Laser Photonics Rev. **14**(10), 2000024 (2020).
6. A. Liu, L. Liao, Y. Chetrit, *et al.*, "Wavelength Division Multiplexing Based Photonic Integrated Circuits on Silicon-on-Insulator Platform," IEEE J. Sel. Top. Quantum Electron. **16**(1), 23–32 (2010).
7. X. Zhou, D. Yi, D. W. U. Chan, *et al.*, "Silicon photonics for high-speed communications and photonic signal processing," npj Nanophotonics **1**(1), 27 (2024).
8. R. Tang, C. Sun, K. Bao, *et al.*, "High-Resolution 2D Quasi-Distributed Optical Sensing with On-Chip Multiplexed FSR-Free Nanobeam Cavity Array," Laser Photonics Rev. **18**(2), 2300828 (2024).
9. L. Li, H. Lin, S. Qiao, *et al.*, "Monolithically integrated stretchable photonics," Light: Sci. Appl. **7**(2), 17138 (2017).

Optical Materials EXPRESS


10. Y. Luo, C. Sun, H. Ma, *et al.*, "Flexible passive integrated photonic devices with superior optical and mechanical performance," Opt. Express **30**(15), 26534–26543 (2022).
11. L. Zhang, L. Jie, M. Zhang, *et al.*, "Ultrahigh-Q silicon racetrack resonators," Photonics Res. **8**(5), 684–689 (2020).
12. Y. Chen, H. Li, and M. Li, "Flexible and tunable silicon photonic circuits on plastic substrates," Sci. Rep. **2**(1), 622 (2012).
13. Z. Chen, Y. Shi, M. Wei, *et al.*, "A Universal Approach to High-Index-Contrast Flexible Integrated Photonics," Adv. Opt. Mater. **11**(9), 2202824 (2023).
14. L. Calvez, "Chalcogenide glasses and glass-ceramics: Transparent materials in the infrared for dual applications," Comptes Rendus. Physique **18**(5-6), 314–322 (2017).
15. J. L. Adam, L. Brilland, P. Toupin, *et al.*, "Chalcogenide glass fibers for photonic devices," in *2013 15th International Conference on Transparent Optical Networks (ICTON)* (2013), pp. 1–4.
16. M. Olivier, J. C. Tchahame, P. Němec, *et al.*, "Structure, nonlinear properties, and photosensitivity of $(GeSe_2)100_{-x}(Sb_2Se_3)_x$ glasses," Opt. Mater. Express **4**(3), 525–540 (2014).
17. R. Qi, W. Zhang, and Y. Huang, "Nonlinear optical properties of chalcogenide glass waveguides fabricated by hot melt smoothing and micro-trench filling," Appl. Phys. Express **13**(4), 042005 (2020).
18. M. Wei, K. Xu, B. Tang, *et al.*, "Monolithic back-end-of-line integration of phase change materials into foundry-manufactured silicon photonics," Nat. Commun. **15**(1), 2786 (2024).
19. J. Hu, V. Tarasov, N. Carlie, *et al.*, "Si-CMOS-compatible lift-off fabrication of low-loss planar chalcogenide waveguides," Opt. Express **15**(19), 11798–11807 (2007).
20. Z. Hu, Y. Li, R. Zhong, *et al.*, "Lithography-Free Chalcogenide Canvas for Photonic Integrated Circuits," ACS Nano **19**(21), 19890–19900 (2025).
21. H. Shang, M. Zhang, D. Sun, *et al.*, "Optical investigation of chalcogenide glass for on-chip integrated devices," Results Phys. **28**, 104552 (2021).
22. M. Pi, C. Zheng, H. Zhao, *et al.*, "Mid-infrared ChG-on-$MgF_2$ waveguide gas sensor based on wavelength modulation spectroscopy," Opt. Lett. **46**(19), 4797–4800 (2021).
23. Z. Han, P. Lin, V. Singh, *et al.*, "On-chip mid-infrared gas detection using chalcogenide glass waveguide," Appl. Phys. Lett. **108**(14), 4945667 (2016).
24. L. Li, Y. Zou, H. Lin, *et al.*, "A Fully-Integrated Flexible Photonic Platform for Chip-to-Chip Optical Interconnects," J. Lightwave Technol. **31**(24), 4080–4086 (2013).
25. S. Serna, H. Lin, C. Alonso-Ramos, *et al.*, "Nonlinear optical properties of integrated GeSbS chalcogenide waveguides," Photonics Res. **6**(5), B37–B42 (2018).
26. S. Dai, F. Chen, Y. Xu, *et al.*, "Mid-infrared optical nonlinearities of chalcogenide glasses in Ge-Sb-Se ternary system," Opt. Express **23**(2), 1300–1307 (2015).
27. P. Janíček, R. Chahal, V. Nazabal, *et al.*, "Temperature-dependent optical functions of selected Ge-Sb-Se bulk chalcogenide glasses obtained by spectroscopic ellipsometry," Ceram. Int. **50**(18), 32812–32817 (2024).
28. F. Han, Y. Niu, Y. Zhang, *et al.*, "Mitigating waveguide loss in Ge–Sb–Se chalcogenide glass photonics," J. Phys. D: Appl. Phys. **57**(30), 305107 (2024).
29. J. Orava, T. Kohoutek, and T. Wagner, "9 - Deposition techniques for chalcogenide thin films," in *Chalcogenide Glasses*, J.-L. Adam and X. Zhang, eds. (Woodhead Publishing, 2014), pp. 265–309.
30. D. Xia, Z. Yang, P. Zeng, *et al.*, "Integrated Chalcogenide Photonics for Microresonator Soliton Combs," Laser Photonics Rev. **17**(3), 2370013 (2023).
31. J. Joule, "The Scientific Papers of Joule JP," London Physical Society **1**, 558 (1884).
32. P. Knotek, P. Kutálek, M. Vlasová, *et al.*, "Ageing of Ge24. 9Sb11. 6S63. 5 thin films under various conditions," Mater. Chem. Phys. **195**, 236–246 (2017).
33. E. A. King, S. Sen, W. Takeda, *et al.*, "Extended aging of Ge-Se glasses below the glass transition temperature," The Journal of Chemical Physics **154**(16), 164502 (2021).
34. R. D. Priestley, "Physical aging of confined glasses," Soft Matter **5**(5), 919–926 (2009).
35. D.-Y. Choi, S. Madden, D. Bulla, *et al.*, "Thermal annealing of arsenic tri-sulphide thin film and its influence on device performance," J. Appl. Phys. **107**(5), 3310803 (2010).
36. Y. Zou, H. Lin, O. Ogbuu, *et al.*, "Effect of annealing conditions on the physio-chemical properties of spin-coated As2Se3 chalcogenide glass films," Opt. Mater. Express **2**(12), 1723–1732 (2012).
37. S. Geiger, Q. Du, B. Huang, *et al.*, "Understanding aging in chalcogenide glass thin films using precision resonant cavity refractometry," Opt. Mater. Express **9**(5), 2252 (2019).
38. Z. Yang, Y. Wang, H. Jin, *et al.*, "Review of chalcogenide glass integrated photonic devices (Invited)," Infrared and Laser Engineering **51**(3), 20220152 (2022).
39. Y. Wang and S. Dai, "Mid-infrared supercontinuum generation in chalcogenide glass fibers: a brief review," PhotoniX **2**(1), 9 (2021).
40. Y. Wang, S. Dai, X. Peng, *et al.*, "Mid-infrared supercontinuum generation spanning from 1.9 to 5.7μm in a chalcogenide fiber taper with ultra-high NA," Infrared Phys. Technol. **88**, 102–105 (2018).
41. Z. Li, C. Hou, Y. Luo, *et al.*, "Embedded racetrack microring resonator sensor based on GeSbSe glasses," Opt. Express **31**(2), 1103–1111 (2023).
42. X. Liu, Y. Tao, X. Zhao, *et al.*, "Complex refractive index sensor based on GeSbSe microring resonator," Opt. Laser Technol. **190**, 112999 (2025).

Optical Materials EXPRESS


43. Q. Du, Z. Luo, H. Zhong, *et al.*, "Chip-scale broadband spectroscopic chemical sensing using an integrated supercontinuum source in a chalcogenide glass waveguide," Photonics Res. **6**(6), 506–510 (2018).
44. J. Pan, Q. Li, Y. Feng, *et al.*, "Parallel interrogation of the chalcogenide-based micro-ring sensor array for photoacoustic tomography," Nat. Commun. **14**(1), 3250 (2023).
45. M. Pi, C. Zheng, H. Zhao, *et al.*, "Ultra-Wideband Mid-Infrared Chalcogenide Suspended Nanorib Waveguide Gas Sensors with Exceptionally High External Confinement Factor beyond Free-Space," ACS Nano **17**(18), 17761–17770 (2023).
46. K. Xia, G. Jia, Y. Guan, *et al.*, "Thermal diffusion preparation and rebonding behavior of Ge20Se80-xTex infrared gradient glass," Ceram. Int. **50**(8), 13318–13326 (2024).
47. Z. Yang, M. Zhao, R. Zhang, *et al.*, "Fabrication of high-Q $Ge_{28}Sb_{12}Se_{60}$ chalcogenide microring resonators in telecommunication band," in *Asia Communications and Photonics Conference/International Conference on Information Photonics and Optical Communications 2020 (ACP/IPOC)*, K. S. D. Xu and L. Wosinska, eds. (Optica Publishing Group, Beijing, 2020), p. M4A.155.
48. X. Zhang, C. Zhou, Y. Luo, *et al.*, "High Q-factor, ultrasensitivity slot microring resonator sensor based on chalcogenide glasses," Opt. Express **30**(3), 3866–3875 (2022).
49. Y. Chen, X. Shen, R. Wang, *et al.*, "Optical and structural properties of Ge–Sb–Se thin films fabricated by sputtering and thermal evaporation," J. Alloys Compd. **548**, 155–160 (2013).
50. L. De Stefano, T. Halenkovič, J. Gutwirth, *et al.*, "Rapid thermal annealing of chalcogenide thin films for mid-infrared sensing and nonlinear photonics," EPJ Web Conf. 309 (2024).